Supporting information for
Temperature-robust diamond magnetometry based on the double-transition method

Caijin Xie,[1,3] Yunbin Zhu,[1,3] Yijin Xie,[1,3] Tingwei Li,[1,3] Wenzhe zhang,[1,3]
Yifan Wang,[1,3] and Xing Rong[1,2,3,*]

[1] *CAS Key Laboratory of Microscale Magnetic Resonance and School of Physical Sciences, University of Science and Technology of China, Hefei 230026, China*
[2] *Hefei National Laboratory, University of Science and Technology of China, Hefei 230088, China*
[3] *CAS Center for Excellence in Quantum Information and Quantum Physics, University of Science and Technology of China, Hefei 230026, China*

* xrong@ustc.edu.cn

I. EXPERIMENTAL SETUP

The diamond sample used in this work was a tool grade (the initial nitrogen concentration between 1∼10 ppm) single crystal chip, grown using chemical vapor deposition (CVD). The diamond was cut into a piece with the size of 1.2 mm × 1.2 mm × 0.4 mm and the 1.2 mm × 1.2 mm facet was perpendicular to the [110] crystal axis. The diamond was irradiated with 3 MeV electrons with 3.16×10^{18} cm^{-2} total flux and subsequently annealed in vacuum at 400 °C, 800 °C and 1000 °C for 2 hours successively.

The 532 nm laser was provided by a high-power optically pumped semiconductor laser (Coherent, Verdi G5). The microwave was generated by a microwave frequency synthesizer (National Instrument, FSW-0010) with the FM option. The AM of microwave was achieved by multiplying the microwave with a modulation signal using an IQ mixer (Marki Microwave, MLIQ-0218L). The modulation signal was provided by a LIA (Zurich Instruments, HF2LI). The attenuator, circulator (Fairview Microwave, SFC0206S) and 20 W amplifier are common configurations. The fluorescence was detected by a PD (Thorlabs, DET36A) and converted to photocurrent after being collected by a CPC (Edmund Optics, #65-441). The photocurrent was sent into the LIA for demodulation. To increase the SNR and protect the LIA, a home-built bias tee was added into the circuit between PD and LIA. The bias tee contained a 2 kΩ resistor to convert the photocurrent into voltage and a 4.7 nF capacitor to block the DC components. It also provided PD with bias voltage.

II. THE PRINCIPLE OF DOUBLE-TRANSITION MAGNETOMETRY

In the double-transition magnetometry, an appropriate magnetic field is applied and the degeneracy of $|m_s = \pm 1\rangle$ states is not completely broken. When using a microwave whose frequency equals to the zero-field splitting D to transfer the population into both of the $|m_s = \pm 1\rangle$ sublevels, each transition between the $|m_s = 0\rangle$ and $|m_s = \pm 1\rangle$ sublevels contributes to the magnetometry signal, and the impacts of D variations induced by temperature drift can be counteracted. For overcoming the flicker noise, the AM of microwave is used to modulate the fluorescence into high frequency domain. The modulated fluorescence is converted to photocurrent and sent into a LIA for demodulation. The demodulated signal serves as the magnetometry signal.

Here, we perform a quantitative analysis for the temperature robustness of double-transition magnetometry and the magnetometry's response to magnetic field.

The AM of microwave is realized by multiplying the microwave with a modulation signal. The function of amplitude modulated microwave can be written as

$$G(t) = \Omega_R[1 + m_a \cos(2\pi\omega_{\mathrm{mod}} t + \phi_{\mathrm{mod}})] \cos(2\pi\omega_d t + \phi_d), \tag{1}$$

where m_a is the amplitude modulation index. Its value is dependent on the amplitude and offset of modulation signal. ω_{mod} and ϕ_{mod} are the frequency and phase of modulation signal. ω_d and ϕ_d are the frequency and phase of microwave.

We assume that the ODMR spectrum of $|m_s = 0\rangle \leftrightarrow |m_s = +1\rangle$ or $|m_s = 0\rangle \leftrightarrow |m_s = -1\rangle$ transition fits the Lorentzian profile [1, 2]. The ODMR spectrum, considering both $|m_s = 0\rangle \leftrightarrow |m_s = \pm 1\rangle$ transitions, can be written as [3]

$$F(\omega) = F_0 \left[1 - \frac{C(\Gamma/2)^2}{(\omega - D + \gamma\alpha B)^2 + (\Gamma/2)^2} - \frac{C(\Gamma/2)^2}{(\omega - D - \gamma\alpha B)^2 + (\Gamma/2)^2}\right]. \tag{2}$$

Where F_0 is the intensity of fluorescence under non-resonance condition. C is the contrast of ODMR spectrum. ω is the microwave frequency. α is the angle factor used for describing the misalignment between magnetic field and the NV symmetry axis [4]. $D = D_0 + \delta D$ is the temperature-dependent zero-field splitting. $B = B_0 + \delta B$ is the strength of magnetic field. D_0 and B_0 are the initial values of D and B, corresponding to $\delta D = 0$ and $\delta B = 0$.

The optimum magnetic field for the double-transition magnetometry is $B_0 = \Gamma/(2\sqrt{3}\gamma\alpha)$, which can realize the optimal temperature robustness and sensitivity simultaneously. We assume that there is $m_a = 1$ in (1). By putting the $\omega = D_0$ and $B_0 = \Gamma/(2\sqrt{3}\gamma\alpha)$ into (2), for a small zero-field splitting variation δD induced by temperature drift and a small magnetic field variation δB, the magnetometry signal is

$$S_{\mathrm{DT}} = -\frac{U_{\mathrm{DT}} F_0 L_0 C}{2} \left\{ \frac{(\Gamma/2)^2}{[\Gamma/(2\sqrt{3}) - \delta D + \gamma\alpha\delta B]^2 + (\Gamma/2)^2} + \frac{(\Gamma/2)^2}{[\Gamma/(2\sqrt{3}) + \delta D + \gamma\alpha\delta B]^2 + (\Gamma/2)^2} \right\}, \tag{3}$$

where U_{DT} is the dimensionless prefactor introduced by the modulation-demodulation protocol for the double-transition magnetometry. Its value is determined by the modulated fluorescence. L_0 is the conversion coefficient between fluorescence and magnetometry signal in voltage units. Its value is determined by the settings of LIA.

Based on (3), the magnetometry signal with $\delta D = 0$, $\delta B = 0$ and $\delta D = \delta B = 0$ can be written as

$$S_{\mathrm{DT}}|_{\delta D=0} \approx -\frac{3U_{\mathrm{DT}}F_0L_0C}{4} + \frac{3\sqrt{3}}{4}\frac{U_{\mathrm{DT}}F_0L_0C}{\Gamma}\gamma\alpha\delta B. \tag{4}$$

$$S_{\mathrm{DT}}|_{\delta B=0} \approx -\frac{3U_{\mathrm{DT}}F_0L_0C}{4} + \frac{27}{4}\frac{U_{\mathrm{DT}}F_0L_0C}{\Gamma^4}(\delta D)^4. \tag{5}$$

$$S_{\mathrm{DT}}|_{\delta D=\delta B=0} = -\frac{3U_{\mathrm{DT}}F_0L_0C}{4}. \tag{6}$$

The taylor expansion is used in the derivation of (4) and (5). According to (5) and (6), the magnetometry signal drift δS induced by δD can be eliminated to the fourth order term in taylor expansion, which is

$$\delta S_{\mathrm{DT}} \approx \frac{27}{4}\frac{U_{\mathrm{DT}}F_0L_0C}{\Gamma^4}(\delta D)^4. \tag{7}$$

Based on (4) and (6), the double-transition magnetometry's maximum slope $|dS/dB|$ in the linear region of magnetometry signal, which represents for the magnetometry's response to magnetic field, can be calculated as

$$\left|\frac{dS_{\mathrm{DT}}}{dB}\right| \approx \frac{3\sqrt{3}}{4}\frac{U_{\mathrm{DT}}F_0L_0C}{\Gamma}\gamma\alpha. \tag{8}$$

It is noteworthy that, due to the NV center electron spin's interaction with crystal stress [5], and the distortion of ODMR spectrum induced by the inhomogeneity of microwave field and magnetic field, the optimum conditon $B_0 = \Gamma/(2\sqrt{3}\gamma\alpha)$ is not strict for the real system. The applied magnetic field was optimized manually in experiment.

As comparison, we also analyse the temperature drift's influence on the conventional diamond magnetometry based on frequency modulated microwave [2, 4, 6], which only utilizes the $|m_s = 0\rangle \leftrightarrow |m_s = +1\rangle$ or $|m_s = 0\rangle \leftrightarrow |m_s = -1\rangle$ transition. For this type of magnetometry (termed here as single-transition magnetometry), a strong bias magnetic field should be applied to break the degeneracy of $|m_s = \pm 1\rangle$ states absolutely. We assume that the center frequency of the frequency modulated microwave equals to the resonance frequency of $|m_s = 0\rangle \leftrightarrow |m_s = +1\rangle$ transition, which is far from the resonance frequency of $|m_s = 0\rangle \leftrightarrow |m_s = -1\rangle$ transition. Considering a small zero-field splitting variation δD and a small magnetic field variation δB, the single-transition magnetometry signal is

$$S_{\mathrm{ST}} \approx -\frac{U_{\mathrm{ST}}F_0L_0C}{2}\left[\frac{(\Gamma/2)^2}{(\omega_{\mathrm{dev}} - \delta D - \gamma\alpha\delta B)^2 + (\Gamma/2)^2} - \frac{(\Gamma/2)^2}{(\omega_{\mathrm{dev}} + \delta D + \gamma\alpha\delta B)^2 + (\Gamma/2)^2}\right], \tag{9}$$

where U_{ST} is the dimensionless prefactor introduced by the modulation-demodulation protocol for the single-transition magnetometry. ω_{dev} is the maximum frequency deviation in the FM of microwave. The optimum condition for the single-transition magnetometry is $\omega_{\mathrm{dev}} = \Gamma/(2\sqrt{3})$.

Based on (9), the single-transition magnetometry signal under optimum condition with $\delta D = 0$, $\delta B = 0$ and $\delta D = \delta B = 0$ can be written as

$$S_{\mathrm{ST}}|_{\delta D=0} \approx -\frac{3\sqrt{3}}{4}\frac{U_{\mathrm{ST}}F_0L_0C}{\Gamma}\gamma\alpha\delta B. \tag{10}$$

$$S_{\mathrm{ST}}|_{\delta B=0} \approx -\frac{3\sqrt{3}}{4}\frac{U_{\mathrm{ST}}F_0L_0C}{\Gamma}\delta D. \tag{11}$$

$$S_{\mathrm{ST}}|_{\delta D=\delta B=0} \approx 0. \tag{12}$$

The taylor expansion is also used in the derivation. According to (11) and (12), for the single-transition magnetometry, the δS induced by δD can be written as

$$\delta S_{\mathrm{ST}} \approx -\frac{3\sqrt{3}}{4}\frac{U_{\mathrm{ST}}F_0L_0C}{\Gamma}\delta D. \tag{13}$$

With the linear relationship between δS and δD, the single-transition magnetometry suffers from the impact of temperature drift.

Based on (8), (10) and (12), the maximum slopes of single-transition and double-transition magnetometry have the same function. The only difference is in the dimensionless prefactors of the two types of magnetometry, which is discussed in the next section.

III. REASONS FOR LOW SENSITIVITY AND FURTHER IMPROVEMENT

The magnetic sensitivity of double-transition magnetometry was demonstrated via the magnetic amplitude spectral density (ASD). Before the computation of ASD, most of the parameters in the experimental setup such as laser and microwave power were optimized.

The maximum slope $|dS/dB|$ was acquired firstly. A stepped magnetic field was applied, and the data in the linear region of magnetometry signal was linearly fitted to get the maximum slope of 636 ± 1 V/T, which is shown in Fig. S1(b).

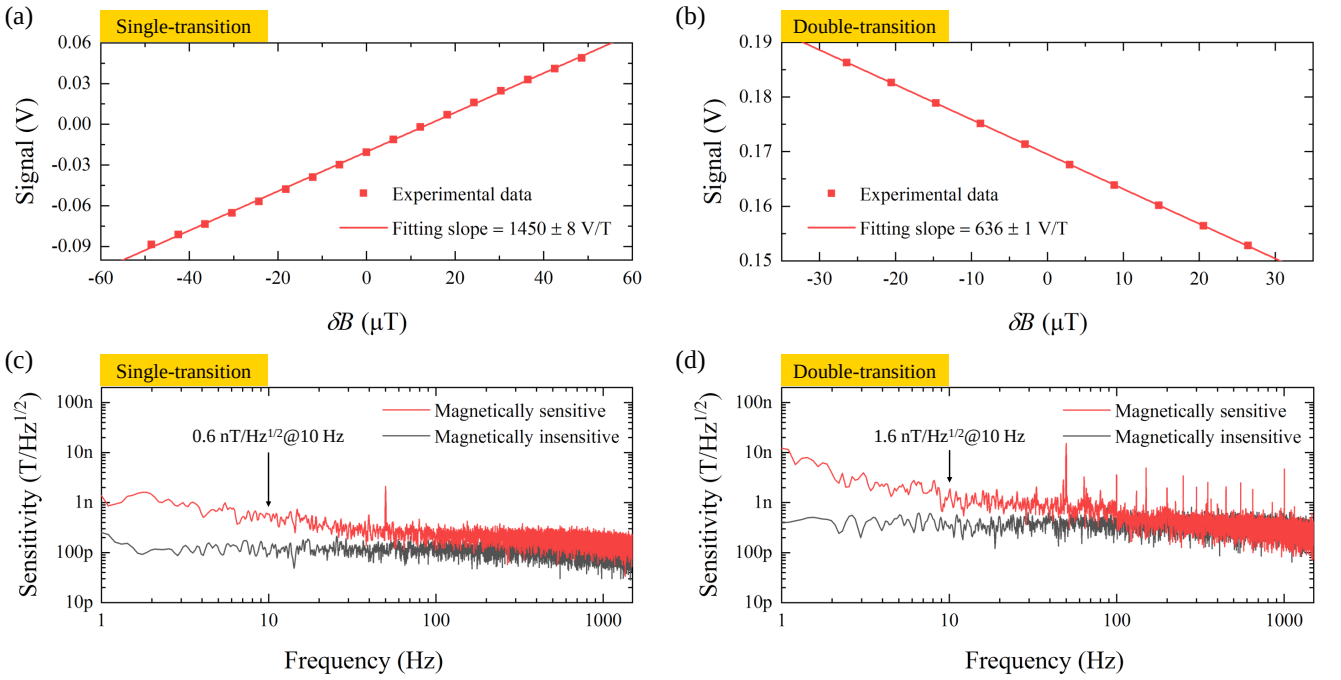

FIG. S1. Maximum slopes $|dS/dB|$ and sensitivities of different types of magnetometry. (a)-(b) The data in the linear regions of magnetometry signals of the single-transition and double-transition magnetometry. (c)-(d) Magnetic amplitude spectral densities of the single-transition and double-transition magnetometry.

Following the method of previous works [4, 7, 8], the time domain magnetometry signals of 20 seconds under magnetically sensitive and insensitive conditions were recorded with sampling rate of 3.6 kHz, and converted to magnetic field units by the $|dS/dB|$. For the double-transition magnetometry, the magnetically insensitive condition was realized by setting the microwave frequency far from the initial value D_0 of zero-field splitting. The ASD was computed using the Welch's method with a 24000-point Blackman-Harris window with 50% overlap, as shown in Fig. S1(d). At 10 Hz, the sensitivity demonstrated by the ASD under magnetically sensitive condition was about 1.6 nT/Hz$^{1/2}$. The noise floor in the range of $1 \sim 1302$ Hz under magnetically insensitive condition was 0.27 ± 0.06 nT/Hz$^{1/2}$.

As comparison, for the single-transition magnetometry, the $|dS/dB|$ was measured as 1450 ± 8 V/T and the sensitivity was demonstrated as 0.6 nT/Hz$^{1/2}$ at 10 Hz. The noise floor in the range of $1 \sim 1302$ Hz under magnetically insensitive condition was 0.11 ± 0.03 nT/Hz$^{1/2}$. The results are shown in Fig. S1(a) and Fig. S1(c). The $|dS/dB|$ and sensitivity of double-transition magnetometry have decreased by 2.3-folds and 2.7-folds respectively, compared with those of the single-transition magnetometry. The main reasons are the decrease of magnetometry signal due to the non-sinusoidal waveform of modulated fluorescence and the noise from the IQ mixer used for AM.

Based on the principle of double-transition magnetometry, the variation of microwave frequency has the same influence on magnetometry signal as the δD, which means the FM of microwave can't be used to modulate the fluorescence. Therefore, we used the AM of microwave to overcome the flicker noise. The variation of microwave field's amplitude will change the contrast C and lead to variation in fluorescence. The contrast can be written as [1]

$$C = \frac{1}{2}\theta \frac{\Gamma_P}{\Gamma_P + \gamma_1^{\mathrm{intr}}(1-\theta)} \frac{(2\pi f_R)^2}{(2\pi f_R)^2 + \gamma_2^{\mathrm{intr}}(\gamma_1^{\mathrm{intr}} + \Gamma_P)}. \tag{14}$$

TABLE I. Parameters used for computation of coefficient between U_{DT} and U_{ST}

Parameter	Value	Reference
m_a	1	Experiment
D_0	2.865 GHz	Experiment
B_0	304 μT (Single-transition) / 194 μT (Double-transition)	Experiment
ω	2.873 GHz (Single-transition) / 2.865 GHz (Double-transition)	Experiment
Γ	13.6 MHz	Experiment
θ	0.09	Experiment
f_R	3 MHz (Single-transition) / $0 \sim 3$ MHz (Double-transition)	Experiment
Γ_P	14.1 MHz	Experiment, [1]
γ_1^{intr}	0.2 kHz	Experiment
γ_2^{intr}	32.8 kHz	Experiment

where θ is the upper limit of contrast. $\gamma_1^{\mathrm{intr}} = 1/T_1^{\mathrm{intr}}$ and $\gamma_2^{\mathrm{intr}} = 1/T_2^{\mathrm{intr}}$ are the intrinsic relaxation rates at room temperature. $\Gamma_P = cP$ is the pump rate, where c is a proportionality constant and P is the power of excitation light [1]. f_R is the rabi frequency, which is in direct proportion to the amplitude of microwave field.

It can be seen from (14) that the relationship between the amplitude of microwave field and C is nonlinear. When the amplitude modulation index m_a is large, which means the amplitude of microwave field changes significantly during the AM process, the waveform of modulated fluorescence will deviate from the sinusoidal waveform severely. Due to the reference signal satisfies the sinusoidal waveform, the dimensionless prefactor of double-transition magnetometry will decrease.

The computed proportionality coefficient between U_{DT} and U_{ST} based on (1), (2) and (14) is $0.52 : 1$. The major parameters used in the computation are listed in Table I. According to (8), the $|dS/dB|$ is in direct proportion to the dimensionless prefactor. As shown in Fig. S1(a)-(b), the proportionality coefficient between the measured $|dS/dB|$ of double-transition and single-transition magnetometry is $0.44 : 1$, which is conformed to the computation.

The decrease of $|dS/dB|$ partly contributed to the decrease of sensitivity. Except for that, since the conventional IQ mixer can suffer from the double-sideband (DSB) noise with $1/f$ behavior [9, 10] which can be brought into the magnetic ASD of double-transition magnetometry, the noise from the IQ mixer used for AM also contributed to the decrease of sensitivity.

The modulation of fluorescence is indispensable for overcoming the flicker noise. According to the discussions above, the modulation-demodulation protocol of double-transition magnetometry must be optimized for further improvement. The reduction of m_a is an approach to suppress the decrease of magnetometry signal caused by the non-sinusoidal waveform of modulated fluorescence. However, it will also reduce the contrast. A better improved scheme is to modulate the fluorescence via the chopping techniques, which have been applied in the field of magnetoresistance sensors for overcoming the intrinsic $1/f$ noise of the sensors [11, 12]. A brief comprehending of the chopping techniques is applying an alternating current (AC) magnetic field on the magnetic sensor to modulate the magnetometry signal into high frequency domain. For the improved scheme that using the chopping techniques, the noise from the IQ mixer vanishes and the decrease of dimensionless prefactor can be overcome.

Based on the derivations in the previous section, we perform a simulation of maximum slope and relationship between magnetometry signal drift and zero-field splitting variation of the improved double-transition magnetometry, and compare with that of the single-transition magnetometry. The results are shown in Fig. S2. With optimized waveform of modulated fluorescence, the maximum slope of improved double-transition magnetometry is approximate to that of the single-transition magnetometry. Besides, the normalized δS of double-transition magnetometry is also immune to δD for the improved scheme.

[1] Jensen, K., Acosta, V., Jarmola, A. & Budker, D. Light narrowing of magnetic resonances in ensembles of nitrogen-vacancy centers in diamond. *Physical review B* **87**, 014115 (2013).

[2] Barry, J. F. *et al.* Optical magnetic detection of single-neuron action potentials using quantum defects in diamond. *Proceedings of the National Academy of Sciences* **113**, 14133–14138 (2016).

[3] Bourgeois, E. *et al.* Photoelectric detection of electron spin resonance of nitrogen-vacancy centres in diamond. *Nature Communications* **6**, 1–8 (2015).

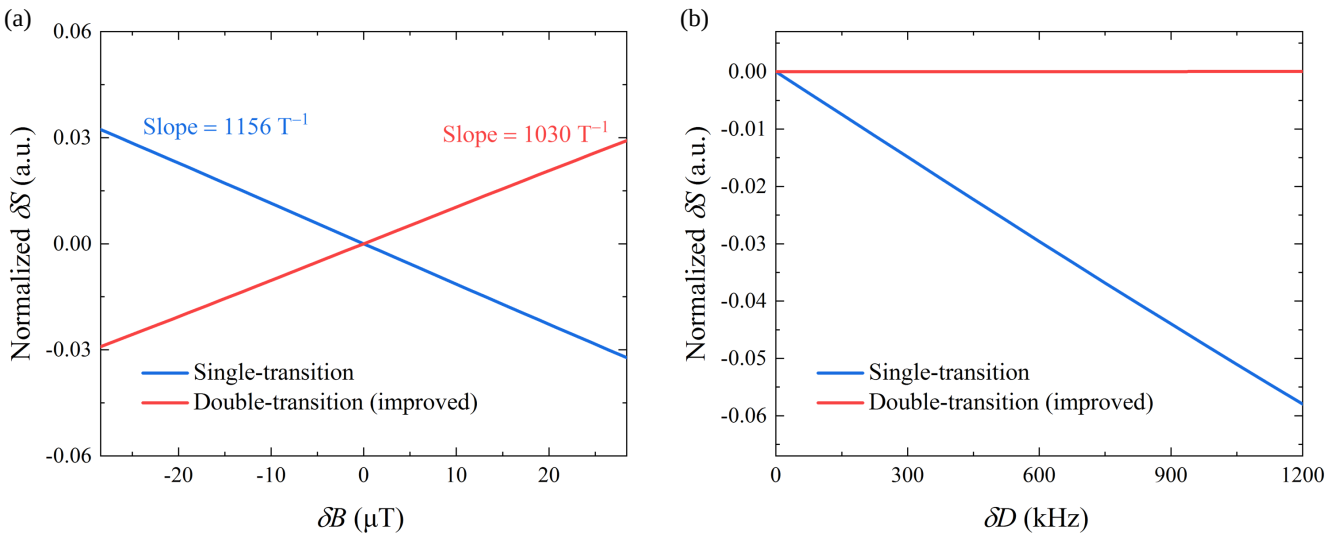

FIG. S2. Simulation results of maximum slopes and relationships between magnetometry signal drift and zero-field splitting variation for the single-transition and improved double-transition magnetometry. (a) Simulation results of maximum slopes for the two types of magnetometry. The δS in ordinate was normallized by setting $F_0 = L_0 = C = 1$. The Γ used in the simulation was set as 15 MHz. (b) Simulation results of relationships between magnetometry signal drift and zero-field splitting variation for the two types of magnetometry.

[4] Xie, Y. *et al.* A hybrid magnetometer towards femtotesla sensitivity under ambient conditions. *Science Bulletin* **66**, 127–132 (2021).

[5] Barry, J. F. *et al.* Sensitivity optimization for nv-diamond magnetometry. *Reviews of Modern Physics* **92**, 015004 (2020).

[6] Clevenson, H. *et al.* Broadband magnetometry and temperature sensing with a light-trapping diamond waveguide. *Nature Physics* **11**, 393–397 (2015).

[7] Zheng, H. *et al.* Zero-field magnetometry based on nitrogen-vacancy ensembles in diamond. *Physical Review Applied* **11**, 064068 (2019).

[8] Fescenko, I. *et al.* Diamond magnetometer enhanced by ferrite flux concentrators. *Physical review research* **2**, 023394 (2020).

[9] Kim, J.-H., An, H.-W. & Yun, T.-Y. A low-noise wlan mixer using switched biasing technique. *IEEE microwave and wireless components letters* **19**, 650–652 (2009).

[10] Lee, J.-S. *et al.* A high linear low flicker noise 25% duty cycle lo i/q mixer for a fm radio receiver. In *2011 IEEE International Symposium of Circuits and Systems (ISCAS)*, 1399–1402 (IEEE, 2011).

[11] Jander, A., Nordman, C., Pohm, A. & Anderson, J. Chopping techniques for low-frequency nanotesla spin-dependent tunneling field sensors. *Journal of applied physics* **93**, 8382–8384 (2003).

[12] Luong, V.-S. *et al.* Reduction of low-frequency noise in tunneling-magnetoresistance sensors with a modulated magnetic shielding. *IEEE Transactions on Magnetics* **50**, 1–4 (2014).